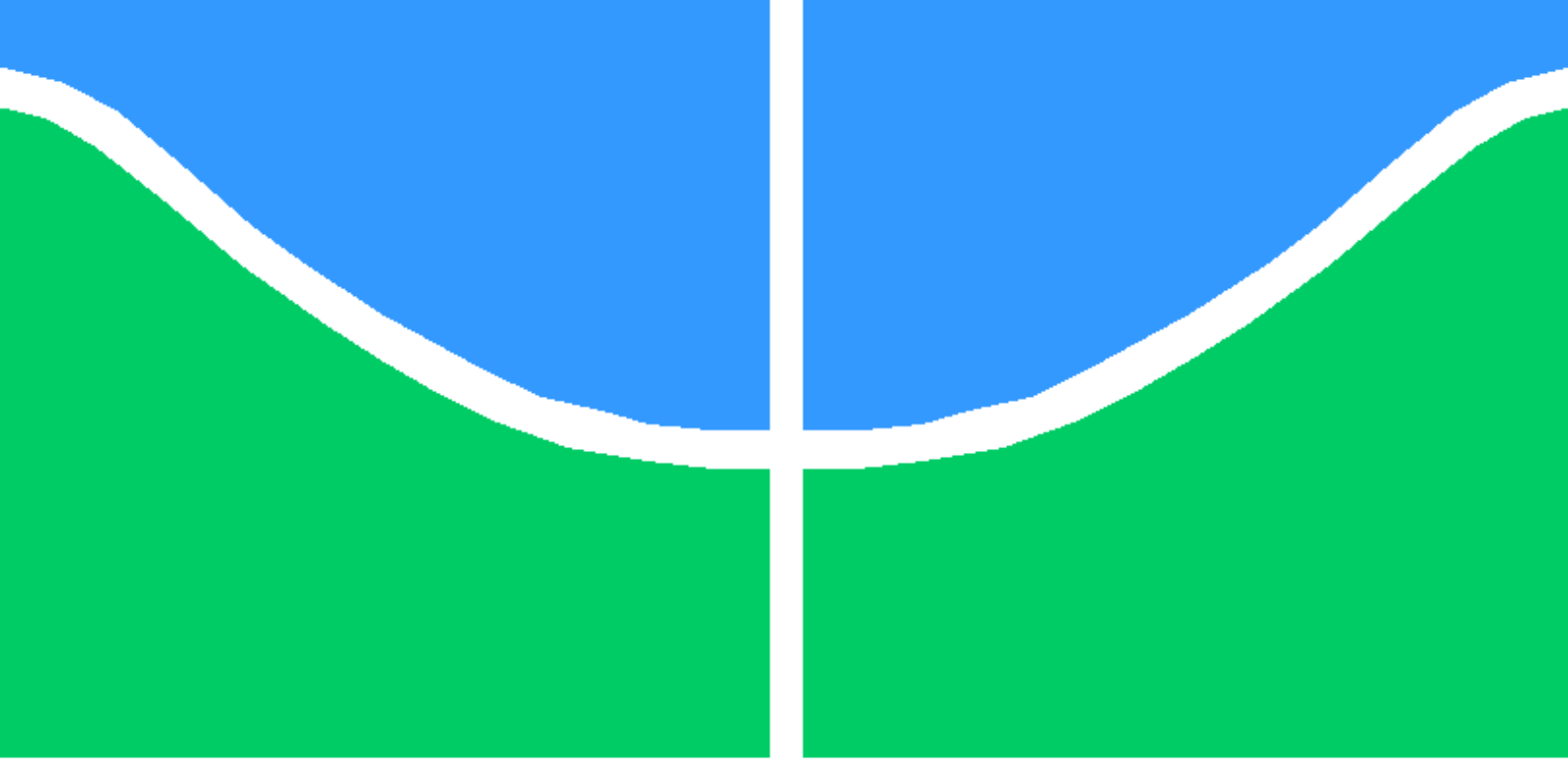

BIO-INSPIRED SMALL WIND TURBINES USING FLYING SEEDS GEOMETRY

BRUNO FRACARO CID DE ALCANTARA

GRADUATION PROJECT IN MECHANICAL ENGINEERING
DEPARTMENT OF MECHANICAL ENGINEERING

FACULDADE DE TECNOLOGIA

UNIVERSIDADE DE BRASÍLIA

UNIVERSIDADE DE BRASÍLIA
FACULDADE DE TECNOLOGIA
DEPARTMENT OF MECHANICAL ENGINEERING

BIO-INSPIRED SMALL WIND TURBINES USING FLYING SEEDS GEOMETRY

BRUNO FRACARO CID DE ALCANTARA

Advisor: PROF. ANTONIO BRASIL JUNIOR, ENM/UNB

GRADUATION PROJECT IN MECHANICAL ENGINEERING

BRASÍLIA-DF, 26 DE JULY DE 2023.

UNIVERSIDADE DE BRASÍLIA
FACULDADE DE TECNOLOGIA
DEPARTMENT OF MECHANICAL ENGINEERING

BIO-INSPIRED SMALL WIND TURBINES USING FLYING SEEDS GEOMETRY

BRUNO FRACARO CID DE ALCANTARA

GRADUATION PROJECT SUBMITED TO THE DEPARTMENT OF MECHANICAL ENGINEERING OF THE FACULDADE DE TECNOLOGIA OF THE UNIVERSIDADE DE BRASÍLIA, AS PART OF THE REQUIREMENTS TO OBTAIN THE DEGREE OF MECHANICAL ENGINEER.

APROVED BY:

Prof. Antonio Brasil Junior, ENM/UnB
Advisor

Prof. Adriano Possebom, ENM/UnB
Internal examiner

Prof. Rafael Mendes, FGA/UnB
Internal examiner

Eng. Matheus Nunes, LEA/UnB
External examiner

BRASÍLIA, 26 DE JULY DE 2023.

CATALOG SHEET
BRUNO FRACARO CID DE ALCANTARA
Bio-inspired small wind turbines using flying seeds geometry
2023xv, 147p., 201x297 mm
(ENM/FT/UnB, Mechanical Engineer, Mechanical Engineering, 2023)
Graduation Project - Universidade de Brasília
Faculdade de Tecnologia - Departamento de Mechanical Engineering

BIBLIOGRAPHIC REFERENCE

BRUNO FRACARO CID DE ALCANTARA (2023) Bio-inspired small wind turbines using flying seeds geometry. Graduation Project em Mechanical Engineering, Department of Mechanical Engineering, Universidade de Brasília, Brasília, DF, 147p.

ASSIGNMENT OF RIGHTS

AUHTOR: Bruno Fracaro Cid de Alcantara
TITLE: Bio-inspired small wind turbines using flying seeds geometry.
DEGREE: Mechanical Engineer YEAR: 2023

_____

Bruno Fracaro Cid de Alcantara
bruno.fracaro.alcantara@gmail.com

Acknowledgment

To my friend and relatives that supported me through the academic journey.

To the LEA team for the technical support in building this project.

Abstract

This study investigates the power coefficient of falling seeds from the *Pterogyne nitens* tree and aims to develop a small wind turbine with blades inspired by the seed's wing-shaped geometry. The study explores the seeds' geometry, structure, fibers, weight, surface characteristics, and flight dynamics to understand their motion and potential for energy generation. High-speed cameras were used to capture the seed's position and inclination during laboratory tests, which provided parameters for rotation and descent. These findings offer insights into the potential for biomimicry in wind turbine design and highlight the importance of understanding natural systems for sustainable energy solutions. This research also presents a study on various turbine models aimed at optimizing the blades and evaluating the power coefficient obtained. Numerical analysis was performed on ANSYS CFX software with the Shear Stress Transport turbulence model and a mesh model designed to accurately reflect the blade/fluid interface and the turbine wake. Several turbine designs were evaluated, varying characteristics such as blade size, pitch angle, and blade surface. The designed blades showed significant differences from traditional models. The blades were tested as flat surfaces, enabling the study of the surface geometry rather than the wing profile. CFD results showed a power coefficient of 0.26 for two turbine models at different configurations, a high torque and low rotation turbine, and a high rotation and low torque turbine. The power coefficient obtained was similar to other turbines developed by the same laboratory with more conventional techniques, this shows that the flying seeds geometry do offer potential for power extraction as wind turbines.

SUMMARY

LIST OF FIGURES

LIST OF TABLES

Chapter 1

Introduction

Flying seeds is one of the essential mechanisms of plant species dispersal. These seeds have specialized structures and natural designs that allow them to travel long distances through the airflow, which helps them to spread to new habitats and establish new colonies. Several examples of flying seeds that use this biological strategy include maples, elms, and cottonwoods [1]-[2].

The structure of containers that allow seeds to fly are varied and ingenious. Some plants, like the maple, have wing-like structures attached to their seeds that help them glide through the air. Others, like the dandelion, have a specialized structure called a *pappus* that acts like a parachute, allowing the seed to be carried in the wind. The designs of these structures have evolved over time, ensuring that the seeds can travel as far as possible to find new habitats which is related to the rate of descent ad its rotating speed [3].

Flying seeds play an essential role in the dispersal of plant species. This process is particularly important in disturbed or changing environments, where plants need to adapt to new habitat conditions. Additionally, flying seeds allow for genetic diversity within a plant species by enabling cross-pollination between different colonies. Overall, the ability of plants to produce flying seeds is a remarkable adaptation that has allowed them to thrive in a wide variety of environments.

The winged seeds, also known as Samaras, have a unique aerodynamic design that allows them to fly through the air and travel significant distances (e.g. [2]), The shape of a samara's wing is crucial to its flight performance, as it needs to generate enough lift to keep the seed aloft while minimizing drag (Figure 1.1). The wings of a samara are typically asymmetrical, with different curved leading and trailing edges. This design allows an adapted airflow over the tilted thin surface, creating a region of low pressure that generates lift in rotatory movement ([4], [5]). As the samaras fly, it will often tilt to one side, causing the wings to spin and further enhance its aerodynamics. Overall, the aerodynamics of samaras is an example of how natural selection has optimized the design of seeds.

Nowadays, the design of small can share some important lessons about the nature evo-

Figure 1.1: Example of Samaras - rotating flying seeds

lution of the aerodynamics of the flying seeds. Aerodynamics efficiency is of utmost relevance in wind turbines as it directly impacts their overall performance and energy output. By maximizing the conversion of wind energy into rotational mechanical energy, efficient aerodynamic design ensures that wind turbines can generate more electricity while operating at lower wind speeds. Improved aerodynamics result in reduced drag, increased lift, and delayed stall, allowing the blades to extract energy from the wind more effectively. Aerodynamics efficiency is particularly relevant in small wind turbines, albeit with some differences compared to larger utility-scale turbines. In small wind turbines, which are typically used for residential or small-scale applications (low Reynolds number), optimizing aerodynamic performance is essential for maximizing energy production within the limited wind resources available. Efficient blade design, incorporating airfoil shapes, twist, and chord length variations, allows small wind turbines to capture more wind energy and convert it into electricity with higher efficiency. By harnessing the available wind resources effectively, aerodynamically efficient small wind turbines offer numerous benefits, including reduced reliance on grid electricity, lower energy costs, and increased sustainability for individual homes, farms, or businesses. Moreover, advancements in small wind turbine aerodynamics contribute to the ongoing development of decentralized renewable energy systems, enabling greater energy independence and resilience at a local level.

Bio-inspired wind turbine design can draw inspiration from natural phenomena and living organisms to enhance the performance and efficiency of wind turbines. Some references has to be discussed this concept as pointed out in [6] and [7]. Other references provide insights into various aspects of bio-inspired wind turbine design, including blade design strategies, optimization techniques, and the potential benefits and challenges associated with integrating bio-inspired principles into wind turbine technology ([8], [9], [10], [11], [12]).

The aim of the present work is to study a small wind turbine concept that utilizes bio-inspiration from samaras for flying aerodynamics. A typical geometry of a flying seed has been selected to design a wind turbine with a rated power of some Watts. This machine is analyzed using a CFD approach.

A micro wind turbine with a diameter of a few centimeters is a compact and efficient renewable energy device designed to capture wind energy on a small scale. With its diminutive size, it can be easily integrated into various applications, such as wearable electronics or

small electronic devices, providing a sustainable power source in portable scenarios. Despite its small dimensions, this micro wind turbine employs advanced aerodynamic principles to maximize power generation from even the slightest air currents. Its lightweight and robust construction make it an ideal solution for powering remote sensors, wireless communication devices, or low-power electronic gadgets in a sustainable and eco-friendly manner. The study for development of those devices, using proper and modern methodologies, can allow efficient machines which can contribute to renewable and sustainable solutions in those scales of application [13], [14], [15], [16], [17].

The present paper is organized as follows: in the next section, the geometry and mechanisms of flight are discussed. Section 3 presents the turbines developed for the study. Section 4 presents the numerical methodology and finally, the last section explores the results and provides a discussion.

Chapter 2

Samaras geometry and flying mechanism

The mechanism of rotating flight of samaras, is often found in tree species such as maples and ashes, which possess a unique ability to spin as they descend. Unlike traditional samaras that rely on passive gliding, these seeds actively rotate around their central axis (highlighted in Figure 2.1c), like miniature helicopters in flight. This spinning motion plays a vital role in their aerial maneuverability and dispersal (see Figure 2.1)

Samaras exhibit a distinct morphology that aids in their flight. Most samaras consist of a central seed surrounded by a wing-like structure (Fig 1.1). The wings are typically flat, elongated, and paired. This form enables samaras to generate lift, slowing their descent and enabling them to travel considerable distances. To achieve their characteristic rotating flight, samaras possess specific structural adaptations. Their wings are often asymmetrical, with one side broader than the other. This design creates an imbalance in the aerodynamic forces acting upon the seed, generating a rotational torque that propels the samaras into a spinning motion. The interaction between air currents and the wing's shape and surface area further enhances the rotation (See Fig. 2.1).

The rotation of samaras is a result of complex aerodynamic principles [18][2]. As the seed descends, the airflow passing over the wings generates varying air pressures on each side due to the wing's asymmetry. This pressure difference creates a force of lift-induced drag, which not only sustains the seed's flight but also drives the rotation. The rotation, in turn, influences the seed's descent rate and horizontal movement. The ability to rotate in flight provides rotating flying samaras with several evolutionary advantages [3].

Samaras exhibit some geometrical characteristics that contribute to their aerodynamic abilities:

- **Wing shape:** The wings of samaras are one of their defining features. Typically, samaras wings have an elongated and flattened shape. The leading edge of the wing is often more rounded, gradually tapering towards the trailing edge. This streamlined shape reduces air resistance and allows for efficient airflow over the surface, enabling sustained flight and reducing drag.

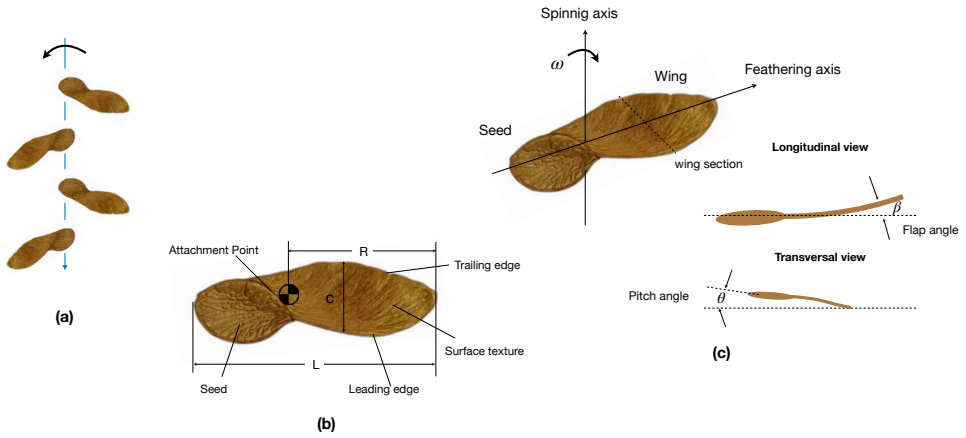

Figure 2.1: Samaras geometry and flying (a) Spinning flying (b) Wing nomenclature (c) Wing design

- **Wing span:** The wing span of samaras varies among different tree species. Some samaras have relatively short wings, while others possess longer wings that extend outward from the central seed. The span of the wings determines the surface area available for generating lift, affecting the duration and distance of the seed's flight. Generally, a larger wing span provides more lift and allows for longer flights and greater dispersal distances.

- **Wing Surface texture:** The surface texture of samara wings also plays a role in their flight characteristics. The wings may have a smooth surface, reducing friction and enabling streamlined airflow (e.g. Pinus). In contrast, some samaras have textured or slightly ribbed surfaces, which can enhance the seed's stability during flight by creating small vortices that help maintain airflow attachment and prevent stalls (e.g. Maple).

- **Wing asymmetry:** In certain samaras, the wings display asymmetry in shape and size. One wing may be broader and longer than the other, resulting in an uneven distribution of forces during flight. This asymmetry induces a rotational motion, causing the samaras to spin as it descends through the air. The rotation enhances stability, aids in maneuverability, and increases the seed's chances of successful dispersal.

- **Seed size and weight:** While the primary focus is often on the wings, the geometrical characteristics of samaras also include the size and weight of the central seed. The seed's dimensions and weight influence the overall balance and flight characteristics of the samaras. Larger seeds tend to have more momentum and may require larger wings to achieve stable flight, while smaller seeds can utilize relatively smaller wings.

- **Seed attachment point:** The location where the wings attach to the seed is another geometrical aspect worth noting. In most samaras, the wings are connected to the seed at one end, often near the top. This attachment point ensures that the wings extend outward and downward, optimizing the lift and stability generated during flight.

Understanding the geometrical characteristics of samaras provides insights into the intricate adaptations nature has developed for effective seed dispersal. The shape, span, surface texture, asymmetry, size, and attachment point of samaras collectively contribute to their flight dynamics, allowing them to navigate the air.

With the purpose of conducting studies on the aerodynamics of samaras and their application in the development of small wind turbines, the chosen species for this research is the "amendoim-bravo" (wild cerrado peanuts). This tree is a native species of the tropical region of South America, belonging to the *Fabaceae* family and scientifically called *Pterogyne nitens*. It is popularly known as "amendoim-bravo" due to the similarity of its seeds to peanuts, but it is important to note that they are extremely toxic for human consumption.

The amendoim-bravo is a perennial shrub that can reach up to 5 meters in height. Its leaves are green and shiny, arranged alternately along the branches. The tree has a spiny stem, with thorns that appear along the branches and trunk. The flowers of the amendoim-bravo are small and greenish, grouped in terminal inflorescences. They usually appear during the rainy season and are pollinated by insects such as bees and butterflies. The plant produces a large number of flowers, which contribute to the formation of fruits. The fruits of the amendoim-bravo are three-lobed capsules that contain seeds inside.

The amendoim-bravo flying seed has evolved to adapt to the conditions of dry habitats in South America, such as the Brazilian cerrado central region. The wind dispersal to more humid areas has promoted the mechanism of flight in this species, and consequently its adaptation. Unlike other species of samaras, the amendoim-bravo the wing design exhibits a curved leading edge, as shown in Fig. 2.1. Its wingspan is short due to the small weight of typical seeds.

Figure 2.2: Amendoim-Bravo (*Pterogyne nitens*) tree and seed containers

Firstly, the geometrical and flying characteristics of the amendoin-bravo have to be determined. A sample of dry seeds is measured to determine the geometrical parameters presented in Table 2.1. A comparison to the *Acer Diabolicum Blume* Maple seed is presented based on the work of Azuma and Yasuda (1989) [3].

Comparing the *Pterogyne nitens* values to those of maple seeds, we observe that *Pterogyne nitens* samaras are longer in length but have a smaller aspect ratio and weigh less. The specimens have an 8% standard deviation of the average, we can consider the specimens

Table 2.1: Samaras geometry characteristics

Parameter	Variable	Amendoim-Bravo	Maple
Length	L	44.1 mm $\pm$ 4.25 mm	36.2 mm
Span	W	12.5 mm $\pm$ 1.44mm	8.4 mm
Weight	m	0.1240 g $\pm$ 0.0206 g	0.58

uniform in their geometrical characteristics, this is favorable to designing a blade with the samara geometry as the blade will be approximate to the samara geometry.

To acquire the precise geometry of the samaras specimens, two scanning methods were used, photogrammetry and scanning through structured light. The second method produced the best results. It was used the David SLS-3 scanner, presented in Figure 2.3, which produced ".stl" files with the 3d scan of the specimen. With the 3d scan, it was possible to develop a 3d CAD model of the samara, that will be later used to build the turbine. The CAD model is shown below in Figure 2.4b.

Figure 2.3: David SLS-3 scanner

((a)) ((b))

Figure 2.4: (a) A photo of the samara. (b) The CAD model of the samara.

Several flight characteristics of the samaras were analyzed and collected. These parameters and their importance is presented here:

- **Falling speed:** Refers to the rate at which the winged seeds descend through the air due to gravity. Understanding the factors that influence falling speed is essential to evaluate the overall flight performance and efficiency of the seeds.
- **Reynolds number at the chord:** Is a dimensionless parameter that relates the flow conditions around the seed to its characteristic dimensions, such as the chord length of the wing. It provides insights into the type of flow regime experienced by the seed, whether it is laminar or turbulent, and influences the aerodynamic forces acting upon it.
- **Angular Rotation:** Plays a significant role in the flight of winged seeds. As they fall, the seeds may experience autorotation, which is a self-sustained rotation due to the interaction between the wing and the airflow. Analyzing the rotation behavior helps determine the stability and descent characteristics of the seeds.
- **Flopping angle:** Refers to the angle between the seed's wing and the horizontal plane. By adjusting the pitch angle, the seed can control its lift and drag forces, affecting its flight trajectory and overall performance.
- **Tip speed ratio:** Is a vital parameter in the study of winged seed flight. It represents the ratio between the linear speed of the seed's wingtip and the incoming wind speed. This parameter determines the efficiency of energy extraction and power generation for winged seeds in wind conditions, providing insights into their optimal operating range.

To measure the flight parameters of the gliding samaras, it was performed experiments in a controlled environment releasing the samaras and observing their glide. The experiment consisted in releasing the samaras in an area with no wind, from a determined height of 2.5 meters, and making the measurements in the bottom 0.5 meters of the fall. To measure the parameters shown in Table 2.2 it was used a speed camera capturing at 960 frames per second, allied with a computer program to measure the samara position at each frame at a given time, and simple calculations to get the parameters in the wanted units. A schematic of the experiment set is presented in Figure 2.5. The camera on top was used to measure the angular velocity and the camera on the side to measure the falling speed and flopping angle.

With the experiment, the flight parameters of interest were collected and are presented in Table 2.2 below. A comparison to the maple seed previously presented is made again.

The falling speed averaged 1,038 m/s, this speed is considered low for the operation of wind turbines, which are optimized to operate for wind speeds above 3 m/s, although we need to account for the small dimensions of a samara when compared to wind turbines. The angular velocity at which the samaras rotate averaged 614 rpm, this value is in the common operational range of small turbines.

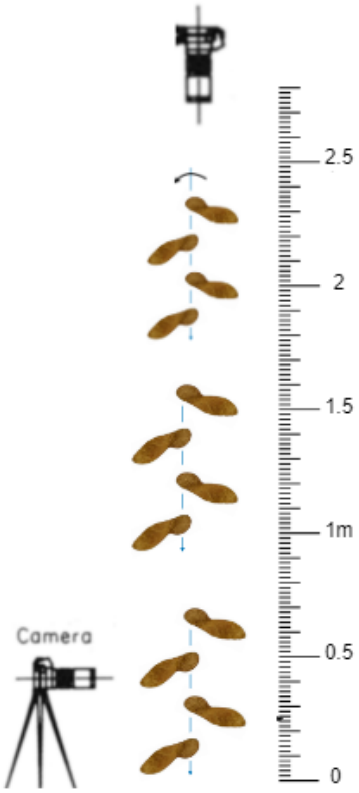

Figure 2.5: Schmeatic of the samaras release experiment

Table 2.2: Flight parameters of the specimens collected

Parameter	**Variable**	**Amendoim-Bravo**	**Maple**
Falling speed	U	1.038 m/s $\pm$ 0.1 m/s	0.82 m/s
Angular velocity	ω	614.797 rpm $\pm$ 56.72 rpm	977 rpm
Reynolds Number at 0.75R	Re	$2.14\times10^3 \pm 0{,}49\times10^3$	1.37×10^3
Tip speed	$R\omega$	2.849 m/s $\pm$ 0.49 m/s	2.91 m/s
Tip speed ratio	TSR	2.77 $\pm$ 0.28	3.57
Flopping angle	β	29.58°$\pm$ 12.71°	23.7°

The top speed ratio was measured as the tip speed divided by the falling speed of the seed. The flopping angle averaged 29,584°, while the pitch angle was very hard to measure due to it being very small, but according to other previous studies is not larger than 2°.

In comparison to the Maple samara, our samaras exhibit a higher falling speed at a lower angular velocity. Despite the maple seed having a higher angular velocity, our samaras maintain a similar tip speed due to their smaller length on the *Acer Diabolicum Blume*.

Armed with this knowledge, we can design a turbine with carefully chosen parameters that enable the blade geometry to effectively harness the wind, mimicking the efficient utilization of wind observed in the samaras.

Chapter 3

Bioinspired micro wind turbine

To develop our bioinspired micro wind turbine, it was used the Inventor Professional 2023 CAD software, from the software house Autodesk Incorporated. This software allowed us to use the “.STL” files obtained from the samara scanning and develop the blade from it.

The turbines were designed around a 41 mm diameter hub with a half sphere with the same diameter as the nose. This hub was selected for being previously used in other studies conducted by the Laboratório de Energia e Ambiente of the Universidade de Brasília, so its effects on the flow are well known. The turbine blades consist of the wing area of the samara. Only the wing area was considered for the blades due to the fact that the seed area does not produce lift for the samara during its falling. The turbine blades were built 2.5 times larger than the actual samaras. This option was made in order to match the seed area to the hub area, making the samara wing the turbine blade. The resulting diameter of the turbines is 206 mm. Multiple turbine models were developed varying their characteristics as the number of blades and pith angle, and evaluated by their power coefficient, as will be discussed further. The turbine model with 8 blades and a 30° pitch angle is shown in Figure 3.1 below:

In order to build the best performing micro turbine with the samaras geometry, multiple turbine models were built, varying the number of blades and their pitch angle, and tested in the CFD software as discussed in the "Methodology" section. All turbine models developed are presented in Table 3.1:

Table 3.1: Turbine models developed

Model	**Blades**	**Pitch angle**
Model 1.1	4	20
Model 1.2	6	20
Model 1.3	8	20
Model 1.4	8	30

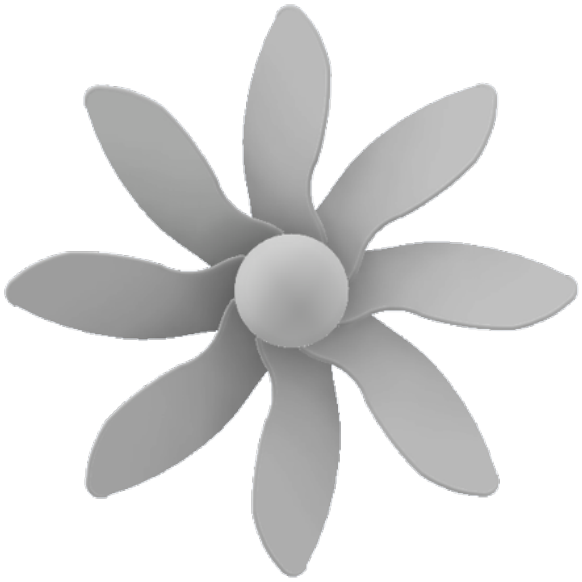

Figure 3.1: CAD image of the Model 1.4 turbine.

As we can see in the table, three models (1.1, 1.2, and 1.3) were built with the same pitch angle of 20°. but increasing the number of blades. After developing Model 1.3, it was noticed that the turbine has a high blade density, prompting the development of Model 1.4 with a different pitch angle to study the effect of this parameter and potentially enhance the power extraction.

Figure 3.2 below shows a 2D CAD of Model 1.4 with its dimensions in millimeters.

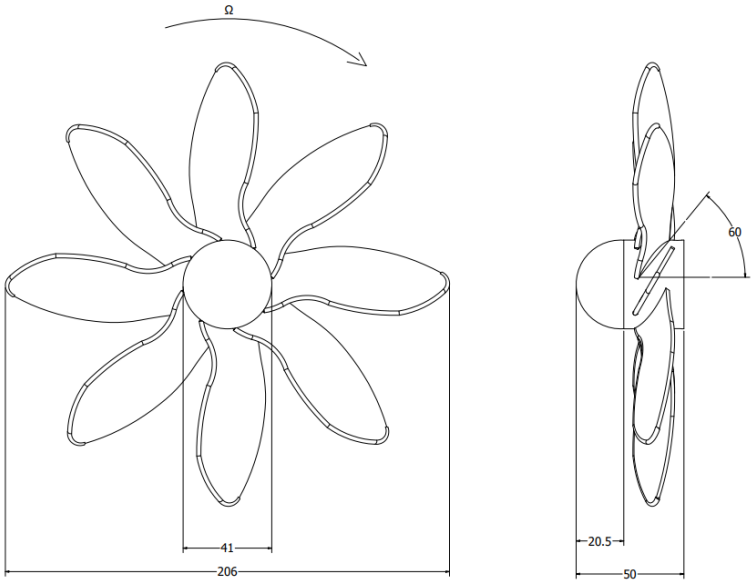

Figure 3.2: Technichal drawing of Model 1.4. Dimensions in mm.

Figure 3.3 shows a 3D rendering of each turbine:

The turbines developed were tested and evaluated regarding their power coefficient. The power coefficient (Cp) is a dimensionless parameter that quantifies the efficiency of energy

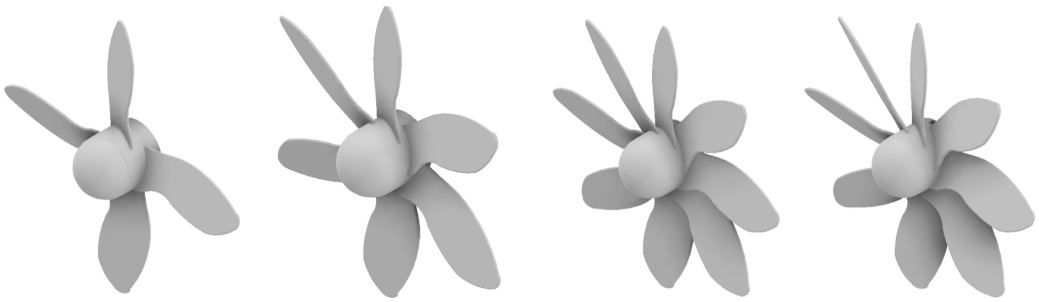

Figure 3.3: From left to right, Model 1.1, Model 1.2, Model 1.3, Model 1.4.

conversion in a wind turbine. It represents the ratio of the actual power output generated by the turbine to the maximum possible power that could be extracted from the wind. The Cp value provides insights into the turbine's ability to capture and convert the wind's kinetic energy into mechanical power. A high Cp value indicates a more efficient turbine that can harness a larger proportion of the available wind energy. It serves as a critical performance metric for assessing and optimizing the efficiency of wind turbine systems. The mathematical description of the power coefficient is given by

$$C_p = \frac{T \times \Omega}{\frac{1}{2} \times \rho \times A \times U_\infty^3},$$

where T is the torque at the rotor in $(N \cdot m)$, Ω is the angular velocity in (rad/s), ρ is the density of the air in (kg/m^3), A is the swept area of the rotor in (m^2) and U_∞ is the wind speed in (m/s).

The turbines can also be evaluated by their generated torque. This is an important information for the selection of components such as generators and bearings. The expression for the torque coefficient is given by

$$C_M = \frac{M}{\frac{1}{2} \times \rho \times A \times U_\infty^2 R},$$

where M is the torque directly calculated by the software in post processing as discussed in the following section.

Another important concept in wind turbine development is the Tip Speed Ratio (TSR), which is a dimensionless parameter used to characterize the rotational speed of a wind turbine rotor in relation to the speed of the incoming wind. It is calculated by dividing the linear speed of the rotor blade tips by the wind speed. The TSR value provides insights into the relative speed at which the blades sweep through the wind, influencing the efficiency and performance of the wind turbine. Higher TSR values indicate a faster rotation of the rotor compared to the wind speed, while lower TSR values imply a slower rotation. The optimal tip speed ratio varies depending on the wind turbine's specific design and operating conditions, with different values providing maximum power capture or enhanced energy

extraction. The expression for the TSR is

$$TSR = \frac{\Omega \times R}{U_\infty}.$$

The power coefficient of horizontal axis wind turbines is strongly related to the tip speed ratio of the turbine. Variations in the flow velocity and angular velocity impact the interaction between the rotor and the fluid, resulting in changes to the generated torque. Therefore, it is customary to analyze the power coefficient in relation to the TSR, adjusting the angular velocity during the design of the turbine and to assess the efficiency of the turbine at the different wind conditions it may encounter. A power curve can be generated by plotting the power coefficient against the tip speed ratio. This curve provides valuable insights into the turbine's maximum performance in terms of power extraction at various rotation speeds. It will be utilized in the methodology section of this study.

Chapter 4

Numerical Setup

Numerical simulations using the CFD method were carried out to evaluate the performance and fluid flow characteristics patterns for typical rotors with variable blade numbers and different pitch angles.

The Ansys CFX software utilizes advanced numerical methods and algorithms to solve the governing equations of fluid dynamics, including the conservation of mass, momentum, and energy. The software employs a finite volume discretization approach, dividing the computational domain into a mesh of cells and solving the equations at discrete points within each cell. This allows for accurate predictions of fluid behavior, such as velocity, pressure, temperature, and turbulence, providing insights into complex flow phenomena. The software also offers a comprehensive suite of tools for pre-processing, simulation setup, post-processing, and visualization, facilitating the analysis and optimization of the turbine models tested.

For the correct simulation on CFX, the software must be configured with the correct inputs and parameters, which shall be discussed in this chapter.

The simulation setup was designed to follow the methodology outlined by [19] but using larger domains and is described in detail here. The outer domain is a parallelepiped, measuring 1.8 meters on each side and 2.25 meters in length, that defines the large fluid region influenced by the turbine. The second one is an immersed cylindrical region, which has a radius of 220 mm and a length of 110 mm, that contains the turbine. In this volume, the flow is described in a rotating reference frame with the same rotation speed of the turbine, in such a way the rotor rotation is taken into account by the action of Coriolis and Centrifugal accelerations. The simulations were performed in a time-dependent flow regime. The arrangement of these domains can be observed in Figures 10a and 10b.

The boundary conditions for the faces of the domains were defined in order to simulate the conditions at which a real turbine would operate without obstructions. The front face of the static domain has the inlet condition with a normal speed directed to the interior of the domain, with a turbulence intensity of 5%. The back face of the static domain has the outlet condition, with an absolute pressure of 0 atm, this forces the fluid to move from the front face

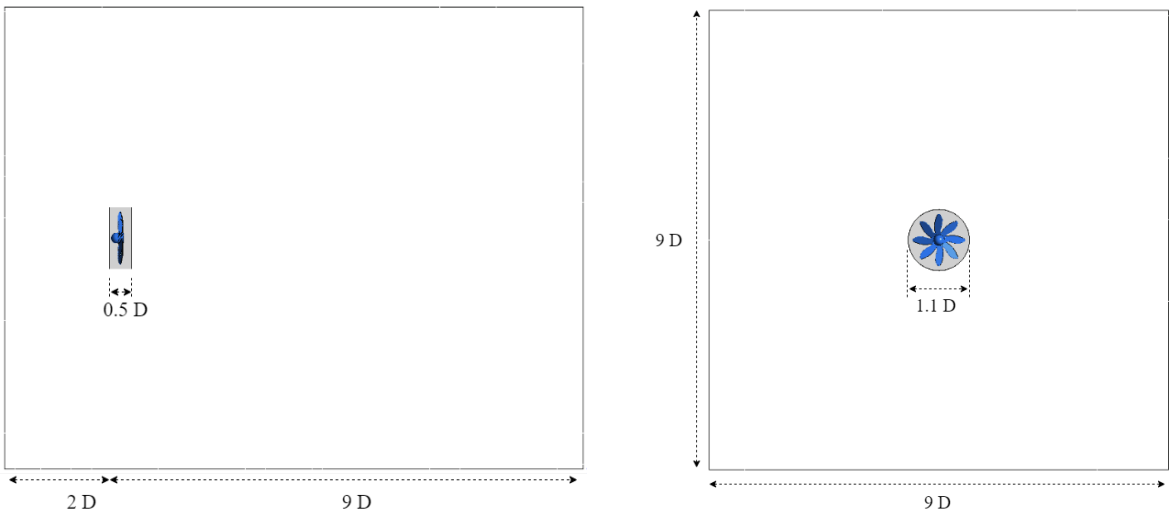

((a)) ((b))

Figure 4.1: (a) Side view of the domains and turbine. (b) Front view of the domains and turbine.

(inlet) to the back face (outlet), with the speed established in the inlet configuration (i.e., 10 meters per second). The sides of the static domain were assigned as opening with a relative pressure of 0 atm, this means that the fluid is free to leave and enter the domain.

The rotor was assigned as a no-slip wall, which means that the fluid directly adjacent to the solid surface has zero velocity relative to the surface, so there is no slip between the rotor and the fluid. The interface of the rotating and stationary domains is assigned as a Transient Frozen Rotor, this setting allows for modeling the time-dependent behavior of the flow while assuming a frozen or fixed rotor geometry that does not deform. It is also determined the inlet velocity for the inlet face and the angular velocity of the rotating domain as values that will vary as shown in the Methodology section. The simulations were performed with the Shear Stress Transport (SST) turbulence model selected due to its accurate results on the near-wall region. The boundary conditions as the whole domain are shown in Figure 4.2.

The mesh was built using a couple of techniques allied with the Ansys Mesh generator. The first technique used was the inflation tool, this tool creates layers of tetrahedral mesh elements around the rotor surface to better capture the boundary layer effect on the blades of the rotor. The quality of the boundary layer has a major impact on the calculation of the local pressure applied on the blades, which impacts the torque at the turbine calculated by the software. The inflation was set as 10 levels with the first layer having a height of 10^4.

The body of influence (BOI) technique was also used for the meshing, this tool allows for the creation of a more refined volume of mesh elements around a region of interest, in this case, the rotating domain and the fluid mat before and after the turbine. This region's refinement is important to achieve a higher precision at the velocity and pressure gradients for the flow. Figure 4.3 shows the 5.8 million nodes mesh with the techniques mentioned.

The mesh size has a direct impact on the precision of the simulation, a more refined

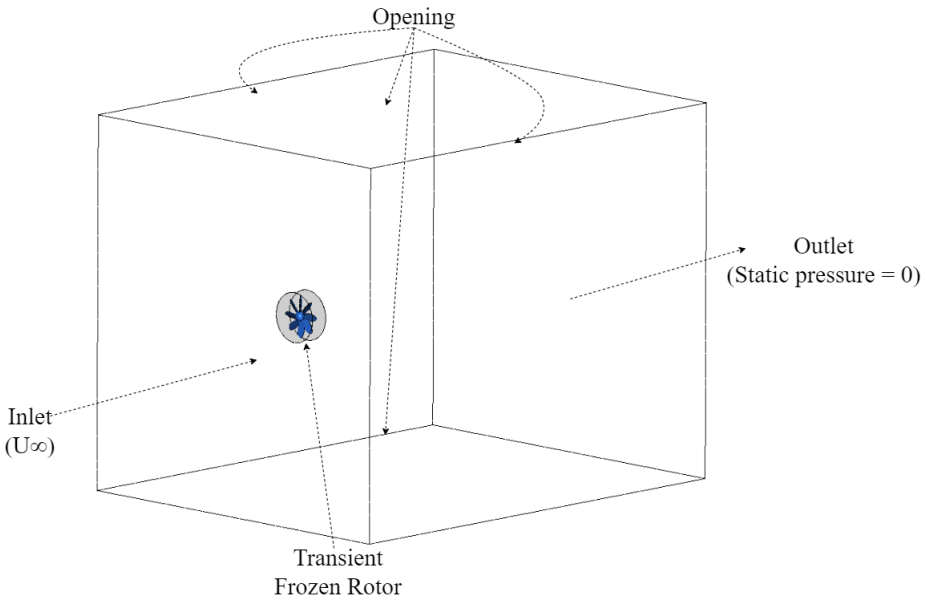

Figure 4.2: 3D view of the surfaces and boundary conditions.

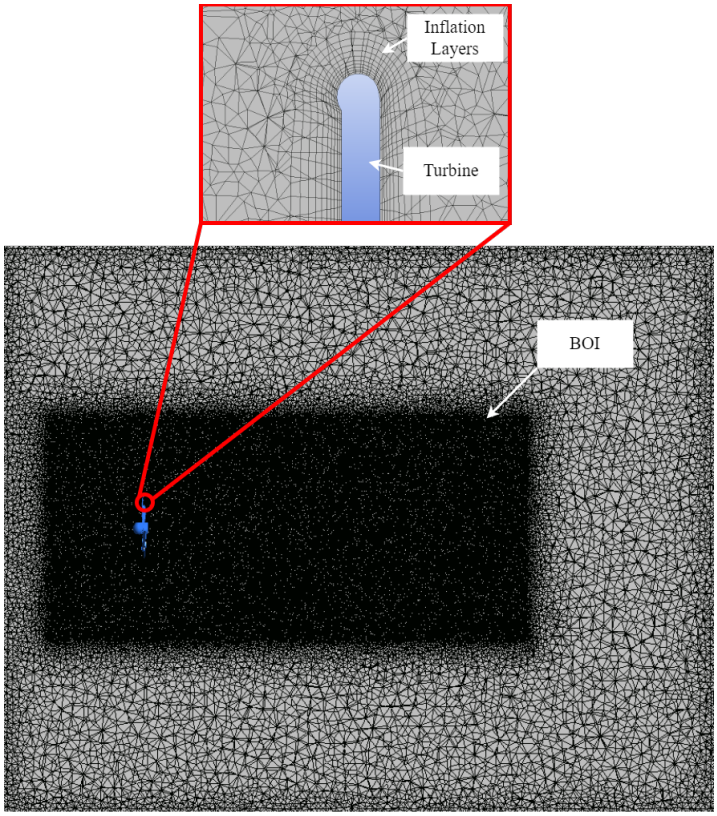

Figure 4.3: Mesh of domains, showing the Body of influence and Inflation Layers

(larger) mesh represents more accurately the real word scenario. A larger mesh also requires more computational power, so it is recommended to perform a mesh convergence study, to assess when the size of the mesh becomes sufficiently good that its increase does not interfere with the torque calculated by the software.

In order to conduct this study, a total of five meshes were created, employing the tools discussed before and reducing the element sizes to enhance accuracy. This refinement re-

sulted in an increased number of elements and nodes within the meshes. Subsequently, the power coefficient was computed for the model 1.4 turbine at 1000 rpm using each mesh configuration. The resulting outcomes are presented in Table 4.1 below.

Table 4.1: Mesh sizes

	Mesh Nodes	C_p
Mesh 1	0.4×10^6	0.166
Mesh 2	1.2×10^6	0.199
Mesh 3	3.5×10^6	0.232
Mesh 4	5.8×10^6	0.242
Mesh 5	7.5×10^6	0.236

The presented table demonstrates a remarkable 42% increase in the power coefficient when transitioning from the roughest mesh (mesh 1) to the more refined mesh (mesh 5), reaffirming the criticality of constructing a well-refined mesh. Additionally, it is worth noting that the calculated power coefficient for mesh 5 was slightly lower than that of mesh 4. It can be assumed that the mesh converged within the range of 5.8 to 7.5 million nodes, and the observed variation is attributed to the larger number of turbine rotations completed before and during the simulation with mesh 5. This increased fidelity of the flow led to a more accurate representation, resulting in a marginally lower power coefficient.

With the objective to assess the effects of the pitch angle and blade number, and select the best turbine model, multiples turbines were built as discussed in the "Bioinspired micro wind turbines" section (Table 3.1). These turbines were simulated in the Ansys CFX software for the same wind speed but varying angular velocities, in order to build the power curve for each model, and verify its maximum power coefficient (as described in the previous section).

This wind speed of 10 m/s was selected as it is considered a good condition for the operation of small and micro wind turbines and is a wind speed that can be tested experimentally in the wind tunnel of the Laboratório de Energia e Ambiente of the Universidade de Brasília in future studies for further validation. The angular velocity range varied for each model. The number of blades influences the tip speed ratio (TSR) at which the turbine achieves its maximum power coefficient (Cp). Therefore, the models with fewer blades, such as Model 1.1 and 1.2, required higher rotation speeds to reach their peak Cp. These conditions resulted in a TSR ranging from 0.7 to 2.6.

The turbines were simulated with the spatial discretization of Mesh 4, as described in Table 4.1.

Chapter 5

Results and discussions

By performing the simulations described in the Numerical Setup section it was possible to build the power curve for the 4 turbine models. The power curves obtained are shown in Figure 5.1:

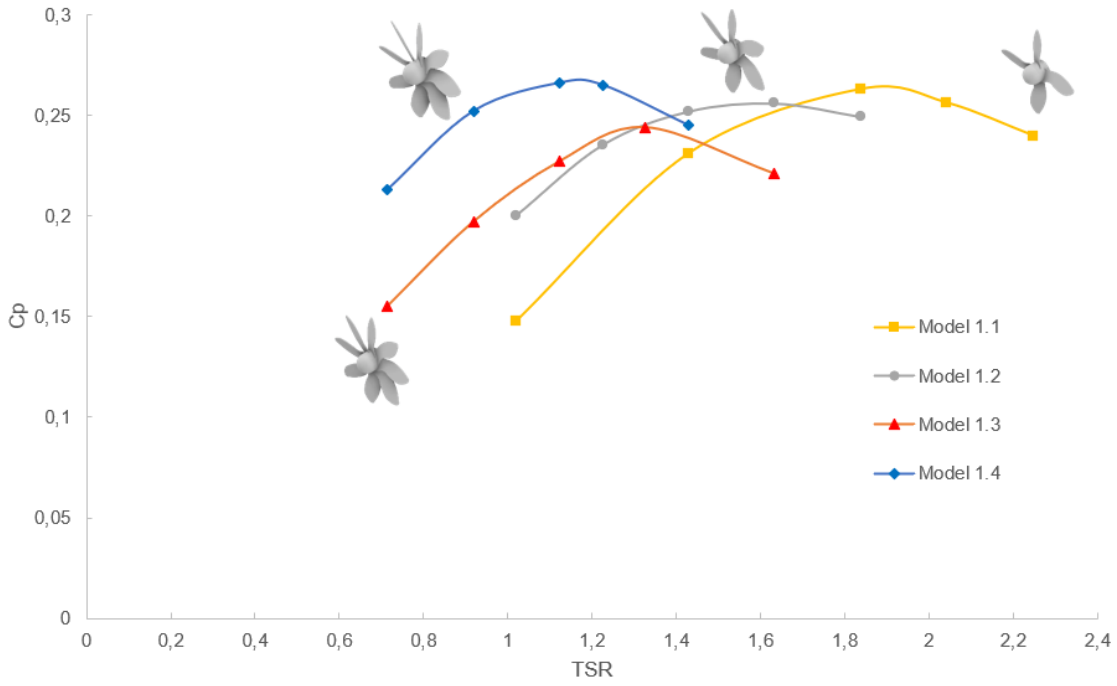

Figure 5.1: Power curves for all models.

As we can see on the chart, models 1.1 (4 blades, 20° pitch angle) and 1.4 (8 blades, 30° pitch angle) achieved the highest power coefficient, at 0.26. This value was achieved at 1.84 TSR (1800 rpm) for the first turbine and at 1.12 TSR (1100 rpm) for the second one, a low value for TSR but in accordance with previous studies of micro wind turbines where the optimum Cp was achieved at lower TSR [7] [20].

Comparing the tree models with the same pitch angle, we can see that the model with fewer blades performed better, and operates at a higher rotation. This confirms the tendency of modern wind turbines to have 3 or 4 blades but goes against previous studies using small

or pico bio-inspired turbines, where a larger blades' number was favorable for the turbine [7].

Comparing the two turbines with 8 blades but different pitch angles, we can notice that the model with the 30° pitch angle performed better at low TSR while achieving a higher maximum CP. This fact indicates that a model with 4 blades and a 30° pitch angle would possibly achieve a power coefficient better than models 1.1 and 1.4.

The turbines with fewer blades exhibited their peak power coefficients at higher TSR, meaning higher rotation speeds. This outcome was anticipated, considering that turbines with fewer blades are capable of achieving faster rotations.

With the torque calculations collected, it is also plotted the torque curve, presented in Figure 5.2;

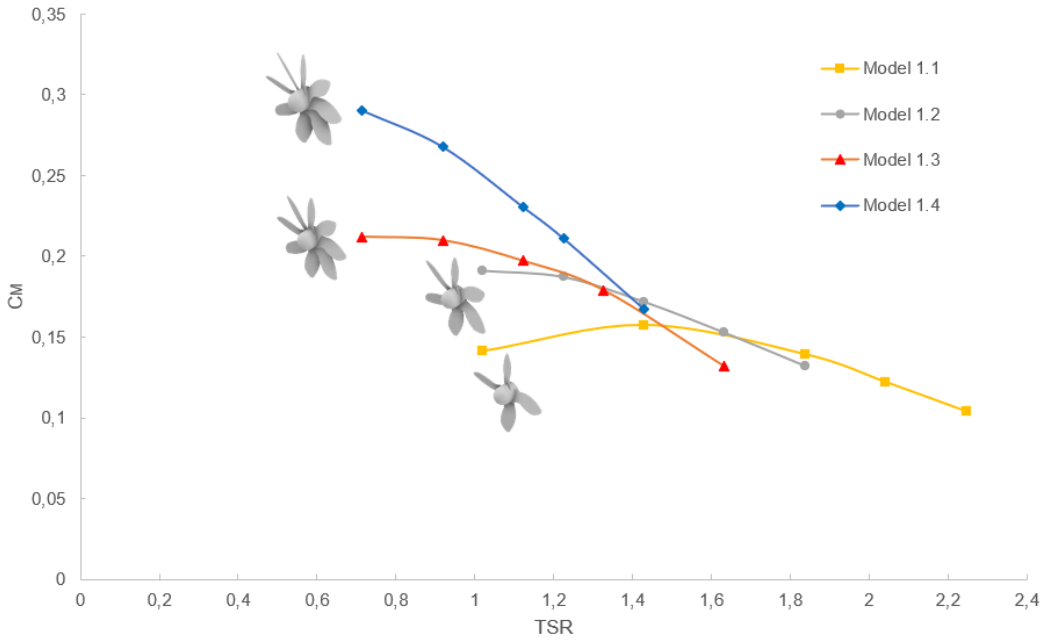

Figure 5.2: Torque curve for all models.

We can see that the turbines with 8 blades generated more torque, which is expected given the larger blade area for the turbine to interact with the fluid. This higher torque comes at a low rotation compared to the model with 4 blades. With this information, we can characterize the two turbine models as having different characteristics but capable of achieving the same power coefficient of 0.26. Model 1.1 (4 blades) operates optimally at high rotation and generates low torque, while model 1.4 (8 blades) operates optimally at low rotation generating high torque.

With the CFD software, more specifically Ansys CFX-Post, it is possible to visualize the flow around the turbine and extract information regarding its operation and the flow conditions around the rotor.

Figures 5.3 and 5.4 provide a qualitative representation of the simulation at 1800 rpm and 10 m/s (1.84 TSR) of model 1.1, showcasing velocity levels and pressure gradients

that demonstrate the physical consistency of the simulated outcomes. These figures reveal distinct hydrodynamic patterns associated with the flow over free axial machines. Notably, the flow behavior upstream of the machine remains consistent until the turbines come into proximity. The interaction between the rotor flow and the surrounding medium generates flow disturbances commonly referred to as a wake, which can be readily observed. The fluid downstream of the turbine experiences a significant decrease in velocity and an increase in turbulence. This can be attributed to the presence of the turbine and its extraction of power from the fluid.

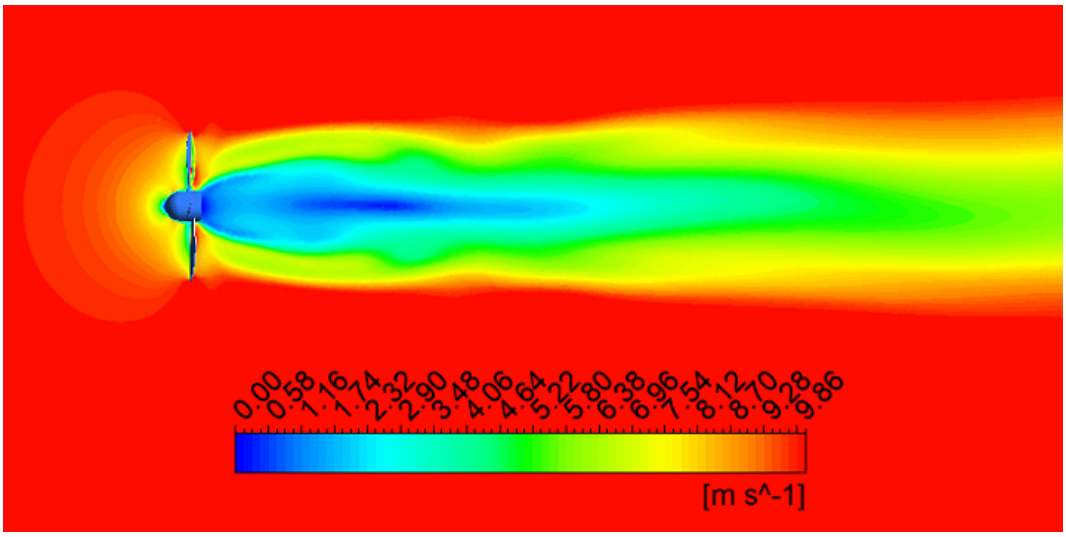

Figure 5.3: Flow velocity contour around Model 1.1.

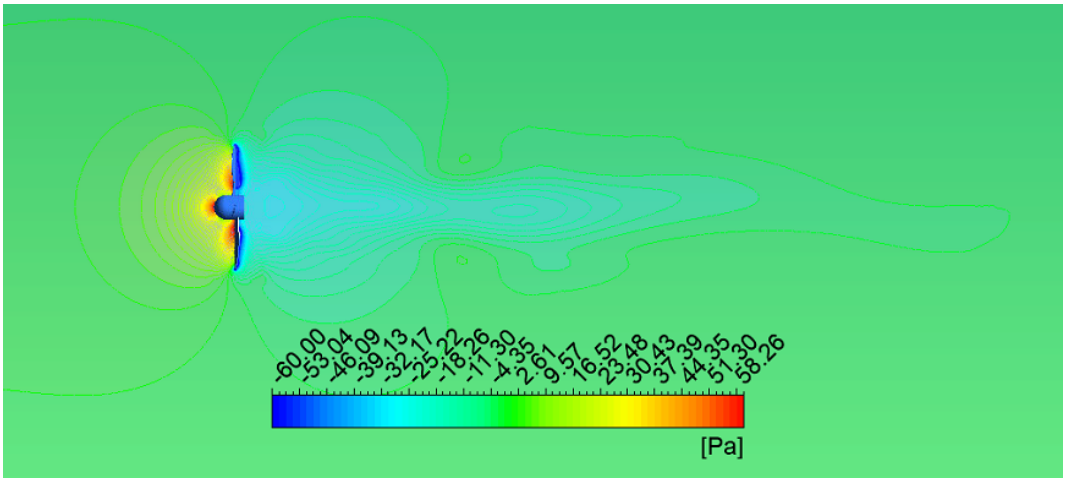

Figure 5.4: Pressure contour around Model 1.1.

In terms of pressure levels, it is observed that there is an increase in pressure ahead of the turbine as a result of its presence, while a lower pressure is observed in the wake of the turbine. This pressure variation is expected and represents the power extraction by the turbine.

Figures 5.5 and 5.6 show the flow for model 1.4 at 1000 rpm and 10 m/s (1.12 TSR).

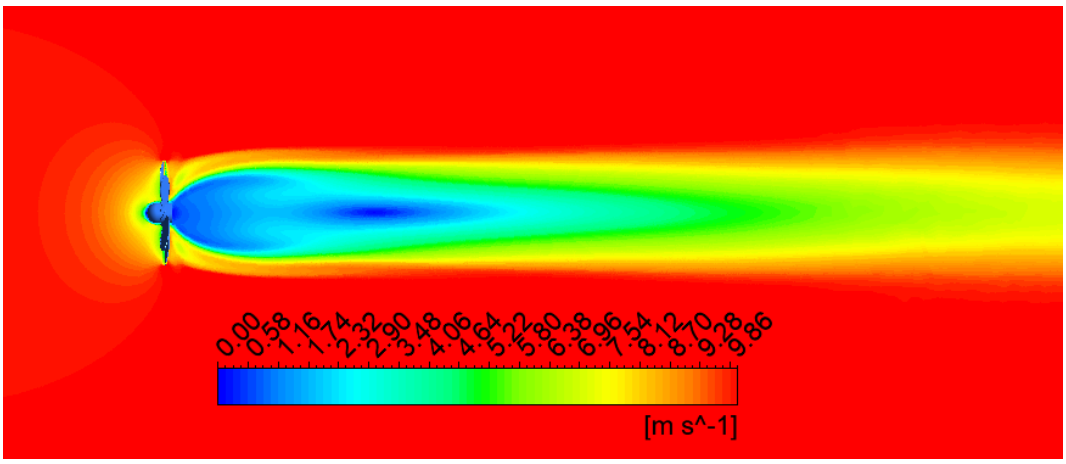

Figure 5.5: Flow velocity contour around Model 1.4.

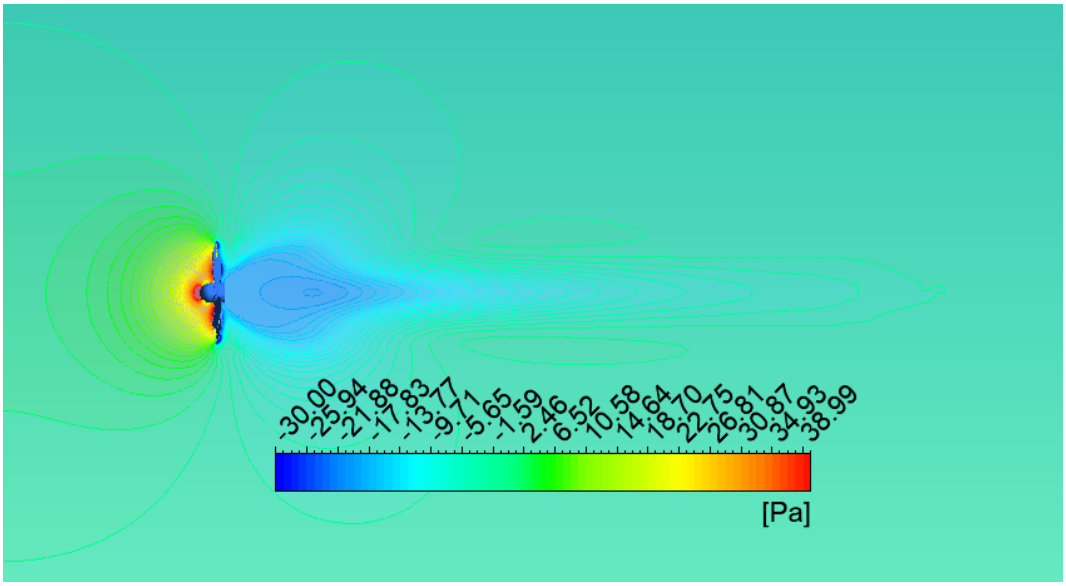

Figure 5.6: Pressure contour around Model 1.4.

Comparing the two velocity contours, we can notice that there is a greater deceleration of the flow in the wake of Model 1.4. This can be attributed to the larger solidity of the turbine, as this one blocks the flow with more intensity due to the larger number of blades.

Regarding the pressure levels, in turbine 1.4, the flow upstream sees a greater influence from the turbine, for the same reason of greater solidity. The induction factor of the turbine with 8 blades is more pronounced, interfering with the flow before the same reaches the turbine, and generating a greater pressure gradient.

The streamlines that run along the surface of the rotor are also a good way to see if there is detachment of the flow that passes in the blade. The goal is for the streamlines to run through the blades without interference and or sections. Figures 5.7 and 5.8 show the streamlines in the intradorsum (left image) and extradorsum (right image) of the blades for the two best models.

It is observed a large recirculation area at the root of Model 1.4 (8 blades), this can be

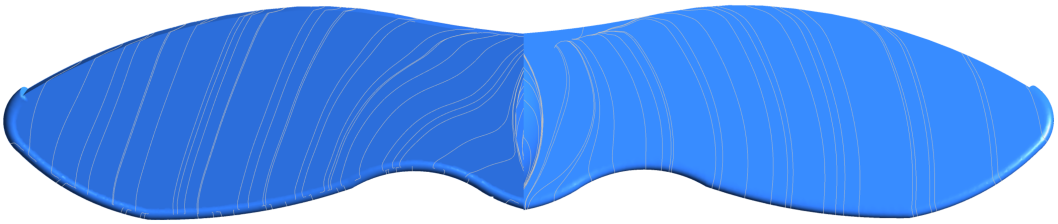

Figure 5.7: Streamlines on the blades of Model 1.1.

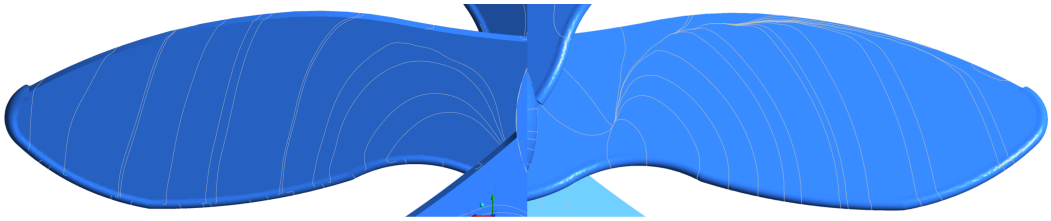

Figure 5.8: Streamlines on the blades of Model 1.4.

attributed to the interference of one blade on the other, as in this section the blades overlap. This is not pronounced in the turbine with 4 blades. Both models see a small detachment of the boundary layer at the trailing edge of the blade, at its root. This is not wanted and could be a focus of improvement or the geometry of the blade.

Chapter 6

Conclusion

This study analyzed the flight of winged seeds from the *Pterogyne nitens* tree to develop bio-inspired wind turbines with blades that resemble the samaras geometry and simulate these turbines using a CFD software.

The experiments conducted with the winged seed specimens provided valuable insights into the flight characteristics and geometry of the samaras, allowing for a comparative analysis with existing literature on samaras. This study enhanced our understanding of the samaras' flight behavior and their similarities and differences with other documented samaras.

The culmination of developing multiple turbines and conducting simulations resulted in the creation of a family of micro wind turbines with a maximum Cp of 0.26 at two different configurations. The model with 8 blades achieved the maximum Cp at a low rotation and high torque, which has been shown to be ideal for small turbines as it helps overtake friction of mechanical parts, while the model with 4 blades achieved the same Cp with much less material at a higher rotation, which can also be desirable depending on the application [20].

The overall performance of the designed turbines can be compared to that of the HK10 turbine developed by the same laboratory of this study but using more conventional blade approaches [19]. In the HydroK project, the HK10 turbine achieved a maximum Cp of 0.25 in wind tunnel testing at a scale model with dimensions similar to the turbines in this study. This value is similar to the Cp achieved here, which demonstrates the effectiveness of samara geometry to interact with the wind despite the absence of common design features like airfoil design or blade twist and generate torque. The findings indicate that samaras hold potential as wind turbine blades for efficient power extraction.

Chapter 7

Next studies

The following areas can be explored as future works:

- **Airfoild profile for blades:** To enhance the power coefficient of the bioinspired blade turbine, it is possible to explore the development of multiple turbines equipped with airfoil profile blades that are renowned for their effectiveness in wind turbines. These turbines can undergo simulation and be compared against the maximum performance attained in this study, thereby enabling an assessment of their potential improvements in power extraction.
- **Wind tunnel experiments:** Verify the correspondence of the simulations to a real-world scenario with experiments of the models in a wind tunnel. The turbine shall be 3D printed and fitted in a hub with a torquimeter to asses its torque generation and make it possible to extract the power curve.
- **Samaras' roughness study:** Develop a method to analyze the effects of the samaras rough surface on its flight. Analyze the usage of the samaras as a wind turbine with its rough surface and compare it to the results obtained without the roughness.

Bibliography

[1] MINAMIA, S.; AZUMA, A. Various flying modes of wind-dispersal seeds. *J Theor Biol*, v. 225, p. 1–14, 2003.

[2] SOHN, M. H.; IM, D. K. Flight characteristics and flow structure of the autorotating maple seeds. *J Visual-japan*, Springer Science and Business Media LLC, v. 25, n. 3, p. 483–500, jan 2022.

[3] AZUMA, A.; YASUDA, K. Flight performance of rotatory seeds. *J. Theor. Biol.*, v. 138, p. 23–53, 1989.

[4] ARRANZ, G. et al. A numerical study of the flow around a model winged seed in autorotation. *Flow, Turbulence and Combustion*, Springer Science and Business Media LLC, v. 101, n. 2, p. 477–497, jul 2018.

[5] CHEN, T.; LAN, S. Numerical analysis of dynamic stability of falling maple samaras. *Acta Mechanica Sinica*, Springer Science and Business Media LLC, v. 38, n. 12, jul 2022.

[6] SIRAM, O.; SAHA, U. K.; SAHOO, N. Blade design considerations of small wind turbines: From classical to emerging bio-inspired profiles/shapes. *Journal of Renewable and Sustainable Energy*, AIP Publishing, v. 14, n. 4, p. 042701, jul 2022.

[7] CARRÉ, A. et al. Extending the operating limits and performances of centimetre-scale wind turbines through biomimicry. *Applied Energy*, Elsevier BV, v. 326, p. 119996, nov 2022.

[8] GAITAN-AROCA, J.; SIERRA, F.; CONTRERAS, J. U. C. Bio-inspired rotor design characterization of a horizontal axis wind turbine. *Energies*, MDPI AG, v. 13, n. 14, p. 3515, jul 2020.

[9] CARRE, A. et al. Innovative blade shape for micro wind turbines. IEEE, jul 2022.

[10] CHU, Y.-J.; LAM, H.-F. Comparative study of the performances of a bio-inspired flexible-bladed wind turbine and a rigid-bladed wind turbine in centimeter-scale. *Energy*, Elsevier BV, v. 213, p. 118835, dec 2020.

[11] HOLDEN, J. R. *Experimental testing and Computational Fluid Dynamics Simulation of Maple Seeds and Performance Analysis as a WInd Turbine*. Dissertação (Mestrado) — University of Cincinnati, 2016.

[12] MAKDAH, A. M. E.; ZHANG, K.; RIVAL, D. E. On the robust autorotation of a samara-inspired rotor in gusty environments. *Bioinspiration and Biomimetics*, IOP Publishing, v. 17, n. 4, p. 044001, may 2022.

[13] TASNEEM, Z. et al. An analytical review on the evaluation of wind resource and wind turbine for urban application: Prospect and challenges. *Developments in the Built Environment*, Elsevier BV, v. 4, p. 100033, nov 2020.

[14] WILBERFORCE, T. et al. Wind turbine concepts for domestic wind power generation at low wind quality sites. *Journal of Cleaner Production*, Elsevier BV, v. 394, p. 136137, mar 2023.

[15] PELLEGRINI, M.; GUZZINI, A.; SACCANI, C. Experimental measurements of the performance of a micro-wind turbine located in an urban area. *Energy Reports*, Elsevier BV, v. 7, p. 3922–3934, nov 2021.

[16] BOURHIS, M.; PEREIRA, M.; RAVELET, F. Experimental investigation of the effect of blade solidity on micro-scale and low tip-speed ratio wind turbines. *Experimental Thermal and Fluid Science*, Elsevier BV, v. 140, p. 110745, jan 2023.

[17] BOURHIS, M.; PEREIRA, M.; RAVELET, F. Experimental investigation of the effects of the reynolds number on the performance and near wake of a wind turbine. *Renewable Energy*, Elsevier BV, v. 209, p. 63–70, jun 2023.

[18] NAVE, G. K. et al. Wind dispersal of natural and biomimetic maple samaras. *Biomimetics*, MDPI AG, v. 6, n. 2, p. 23, mar 2021.

[19] JUNIOR, A. C. P. B. et al. Hydrokinetic propeller turbines. How many blades? *American Journal of Hydropower, Water and Environment Systems*, Centro Nacional de Referência em Pequenas Centrais Hidrelétricas, UNIFEI, v. 2, p. 16–23, jun. 2017.

[20] BOURHIS, M. et al. Innovative design method and experimental investigation of a small-scale and very low tip-speed ratio wind turbine. *Experimental Thermal and Fluid Science*, v. 130, p. 110504, 2022. ISSN 0894-1777.